Relevant Synthesis Parameters for the Sequential Catalytic Growth of Carbon Nanotubes

Vincent Jourdain,*,† Matthieu Paillet,† Robert Almairac,† Annick Loiseau,‡ and Patrick Bernier†

GDPC, Université Montpellier II, Place Eugène Bataillon, CC26, 34095 Montpellier Cedex 5, France, and LEM, UMR 104 CNRS-ONERA, ONERA, BP 72, 92322 Châtillon Cedex, France

Received: July 29, 2004; In Final Form: November 4, 2004

Sequential catalytic growth provides an efficient tool for the synthesis of carbon nanotubes periodically inserted with catalyst nanoparticles. Several synthesis parameters were found crucial in order to induce this particular growth mechanism. The presence of phosphorus is required to form metal phosphide particles active for the formation of carbon nanotubes with a matchstick morphology. The metal composition (Ni/Fe ratio) and the carbon supply have no influence on the nanofilament type but strongly affect the nanotube yield. The synthesis temperature induces important changes on both the nanofilament type and yield, which are correlated with important transformations of the catalyst layer in terms of composition, particle size, and physical state.

Introduction

Because of their exceptional electric, mechanical, and structural properties, carbon nanotubes are promising materials for a wide range of applications such as electron field emitters,[1,2] electronic nanodevices,[3−5] and nanomachine components.[6,7] Moreover, the possibility of filling their inner channel with foreign materials opens the way to the design of new hybrid materials with novel or enhanced properties, in terms of electron charge transport,[8] spin transport,[9,10] magnetic storage,[11] and so forth. In as early as 1992, theoretical studies predicted that, at normal pressure, a liquid with a surface tension of <200 mN m^{-1} would spontaneously fill the nanotube inner channel.[12,13] Since that moment, two types of methods have been used: in situ filling during the nanotube growth[14−19] and post situ filling by postgrowth opening of the nanotubes.[12,20−22] Numerous compounds and elements were quite successfully inserted in the nanotube inner channel by these two methods. In 2000, sulfur was shown to promote the filling of the nanotubes with metals and metal sulfides.[23] However, a major drawback for the design of more complex hybrid nanostructures lies in the impossibility of controlling the location and length of the filling domains.

Our group recently discovered and studied an original growth mode enabling carbon nanotubes to be periodically inserted with catalyst nanoparticles during their growth.[24,25] We showed that using phosphorus as a cocatalyst enables one to induce periodic initiations and interruptions of the growth with the insertion of a fraction of the catalyst particle at each new initiation. This mechanism was so-called "sequential catalytic growth". The as-produced nanofilaments were named "matchstick nanotubes" because of the shape of their elementary units. One particular interest lies in the possibility of inserting small (usually monocrystalline) and separated particles along the whole length of the carbon nanofilament. The resulting nanostructures could find applications in magnetic storage and nanospintronics. Until now, the nanoparticles inserted in these matchstick nanotubes were only nickel iron phosphides, but other metal phosphides or sulfides could be envisioned. In that perspective, we report here on the synthesis parameters found critical in order to induce the sequential catalytic growth of carbon nanotubes in the case of Ni/Fe/P catalyst particles. These include both the catalyst system (catalyst support, particle composition, size, and physical state) and the growth conditions (temperature and carbon supply). The influence of the different parameters on the formation of the active catalyst particles and the matchstick nanotubes is discussed.

Experimental Section

Catalyst Preparation. Layers of nickel, iron, and cobalt were deposited by evaporation on different flat catalyst supports: silicon, silica, alumina (Alfa Aesar, single crystal, 99.9%), phosphoric acid-impregnated alumina, and anodic alumina membranes (AAMs, Anodisc Whatman, 0.02 μm). AAMs intrinsically contain $\sim$1.5 atom % phosphorus due to the phosphoric acid used during their synthesis. The layer thickness was controlled by an in situ quartz balance.

Synthesis. The supported catalysts were heated at 10 °C/min in air until 600 °C and under argon flow until the growth temperature (880−1160 °C). A CH_4/H_2 gas mixture was introduced into the reactor for 5 min. The influence of the CH_4 flow rate was studied in the range 36−300 sccm, while keeping the H_2 flow rate constant at 730 sccm. The reactive species were purged for 15 min with an argon flow before the reactor was allowed to cool.

Characterization. The evolution of the crystal structure of the supported catalyst layer with the temperature was investigated by X-ray diffraction (XRD) (INEL CPS120, Cu Kα). The nanofilaments were characterized by scanning electron microscopy (SEM) (Hitachi S-4500), transmission electron microscopy (TEM) (JEOL 1200 EX2, 100 kV), and high-resolution TEM (HRTEM) (Philips, CM20, 200 kV). The TEM grids were prepared by wetting in ethanol suspensions obtained by ultrasonication of the supports. The nanoparticle composition was determined by localized energy-dispersive X-ray spectroscopy (EDX) in a high-resolution transmission electron microscope (Philips, CM20, 200 kV).

* Corresponding author. Phone: +33 4 67 14 35 29. Fax: +33 4 67 52 25 04. E-mail: jourdain@gdpc.univ-montp2.fr.
† Université Montpellier II.
‡ UMR 104 CNRS-ONERA.

10.1021/jp046619v CCC: $30.25
Published on Web 01/08/2005

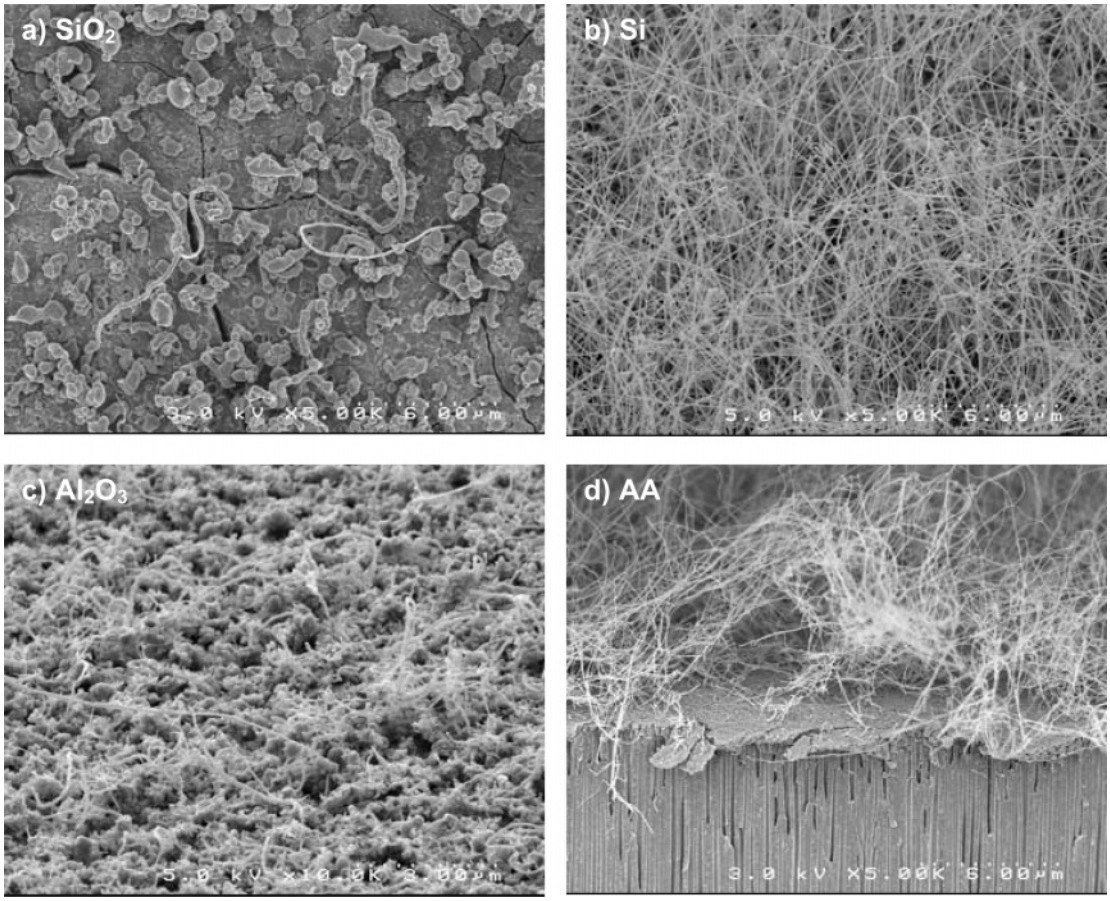

Figure 1. Postsynthesis SEM images of the Ni/Fe catalyst supported on (a) silica, (b) silicon, (c) pure alumina, and (d) anodic alumina (AA).

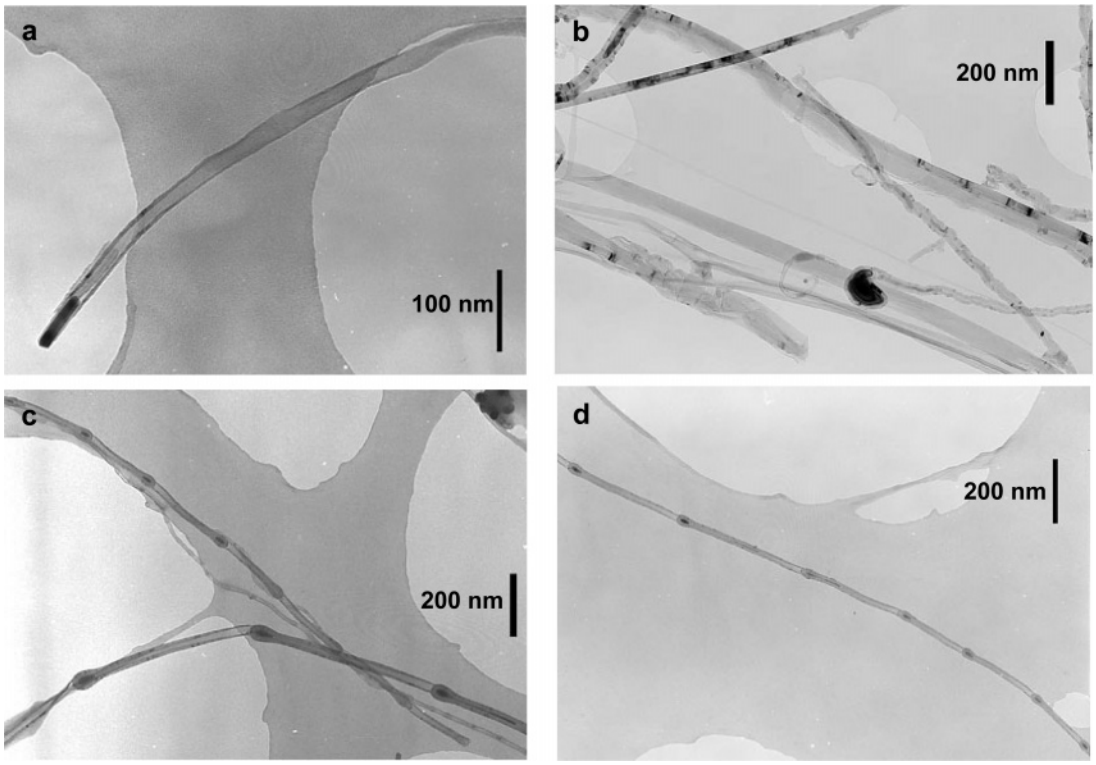

Figure 2. TEM images of the nanofilaments grown with Ni/Fe catalyst supported on (a) silicon, (b) pure alumina, (c) anodic alumina, and (d) phosphoric acid-impregnated alumina.

Results and Discussion

Influence of the Catalyst. During this study, the growth conditions were kept constant: 1080 °C, 100 sccm CH_4/730 sccm H_2. The catalytic activity of the supported catalysts for nanofilament growth was evaluated by postsynthesis SEM observation of the substrates.

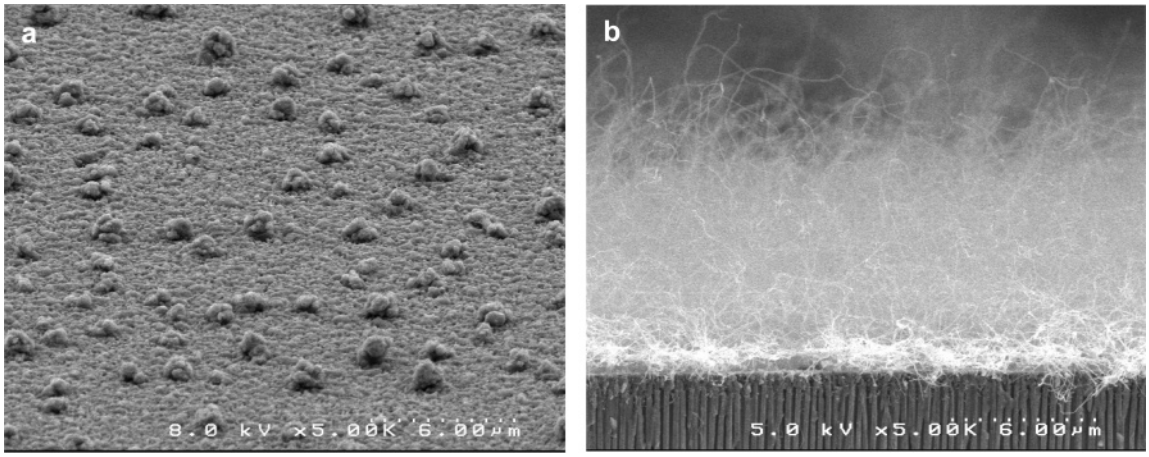

Figure 3. Postsynthesis SEM images for different anodic-alumina-supported catalysts: (a) 100 nm Fe; (b) 88 nm Ni/30 nm Fe.

a. Catalyst Support. The influence of the nature of the catalyst support was investigated while keeping constant the deposited catalyst proportions at 64 nm Ni/15 nm Fe. Figure 1 shows postsynthesis SEM images for different catalyst supports: silica, silicon, pure alumina, and anodic alumina. Nearly no filaments are grown on silica. Silicon shows an excellent catalytic activity with the formation of a dense entanglement of very straight nanofilaments. Pure alumina presents quite a low catalytic activity characterized by the formation of diverse and disordered nanostructures. Anodic alumina gives a high catalytic activity with the abundant formation of entangled and tortuous nanofilaments.

TEM (Figure 2a−c) allowed the nature of the nanofilaments grown on each support to be precisely characterized. Only quite straight multiwall carbon nanotubes without metal inclusion are grown on silicon. Disordered and partially filled filaments of various shapes and diameters are grown on pure alumina. On the contrary, anodic alumina selectively induces the formation of matchstick nanotubes with characteristic nanoparticle periodic inclusions along their whole length. Compared to pure alumina, anodic alumina is characterized by a noticeable phosphorus content (∼1.5 atom %) resulting from the phosphoric acid used during its synthesis. We formerly reported that a significant amount of phosphorus (∼27 atom %) was found in the composition of the nanoparticles inserted in the nanomatches.[25] We demonstrated that adding phosphorus to pure alumina (by impregnation in 15 M phosphoric acid) enabled us to reproduce the results obtained with anodic alumina, that is, the selective formation of matchstick nanotubes (Figure 2d).

These results show that, in the absence of phosphorus, diverse types of carbon nanostructures (straight multiwall nanotubes and disordered and partially filled nanofilaments) can be formed depending on the nature of the catalyst support. We confirm that the presence of phosphorus in the catalyst phase is needed for the formation of matchstick nanotubes: phosphorus can be intrinsically present in the support or extrinsically added (by subsequent phosphoric acid impregnation, for instance). Controlling the phosphorus content in the catalyst phase and studying its influence on the catalytic activity is under progress.

b. Nature and Proportions of the Deposited Catalyst. The influence of the nature and proportions of the deposited catalysts (Ni, Fe, Co, Ni/Fe, and Co/Fe with typical thicknesses of <100 nm) was studied using anodic alumina as the catalyst support. Under the growth conditions used herein (see above), pure elements (Ni, Fe, and Co) and mixed Co/Fe layers showed no or very low catalytic activities, whatever the deposited thickness (see, for instance, Figure 3a for a 100 nm Fe layer). On the contrary, mixed Ni/Fe layers were found to effectively promote the formation of matchstick nanotubes (Figure 3b). A systematic study of the influence of the Ni/Fe proportions on the catalytic activity is presented in Figure 4. Best activities are generally observed for mixed Ni/Fe catalysts with a high Ni content. We highlight that only nanotubes of the matchstick type were grown under the conditions used herein, whatever the nature and proportions of the deposited catalyst layer.

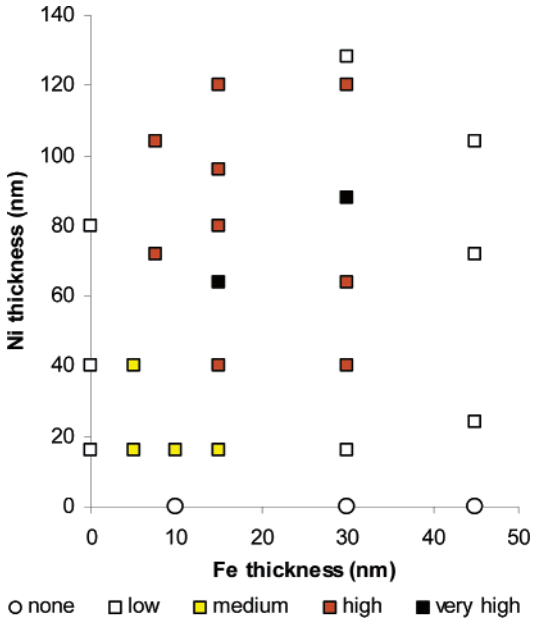

Figure 4. Catalytic activity as a function of the Ni and Fe thickness.

The following conclusions can be drawn from these results: (a) the matchstick morphology is independent of the nature and proportions of the deposited metal catalysts, provided that phosphorus is present; (b) the catalytic activity and thus the nanotube yield are strongly influenced by the nature and proportions of the deposited metal catalysts. Obviously, the metal nature and proportions are key parameters for forming active nucleation seeds for the growth of matchstick nanotubes. Our previous investigations demonstrated that these active catalyst particles have several important features: they are metal phosphide particles, in a fluid state, with typical initial diameters of <80 nm.[25] In the phosphorus concentration (x_P) range we are interested in (∼27 atom %), the Ni/P, Co/P, and Fe/P binary diagrams are quite similar with a characteristic eutectic point at $x_P \sim 17-20$ atom %.[26] The main difference consists of the eutectic temperature: 870 °C for Ni/P, 1023 °C for Co/P, and

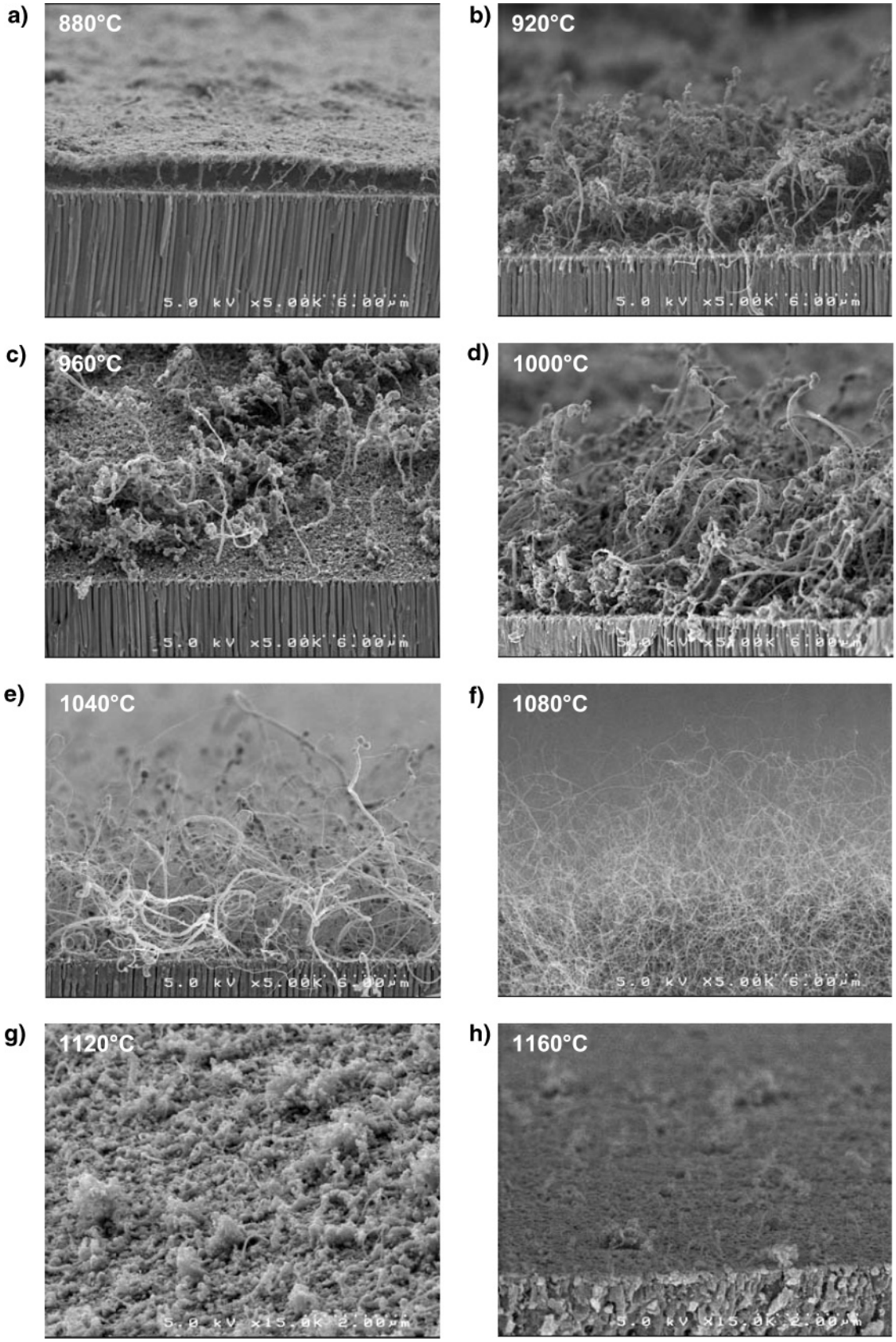

Figure 5. Postsynthesis SEM images of the substrate for different synthesis temperatures.

1048 °C for Fe/P. Assuming that the relative difference of eutectic temperatures is conserved even for 20−80 nm particles, we should conclude that liquid droplets of Ni phosphide, and presumably of Ni-rich metal phosphide, start forming at much lower temperatures than in case of the Co/P or Fe/P systems. The difference in catalytic activity with the catalyst nature and proportions could then be interpreted in terms of different formation temperatures of small liquid metal phosphide particles. If so, the synthesis temperature should significantly affect the growth of matchstick nanotubes.

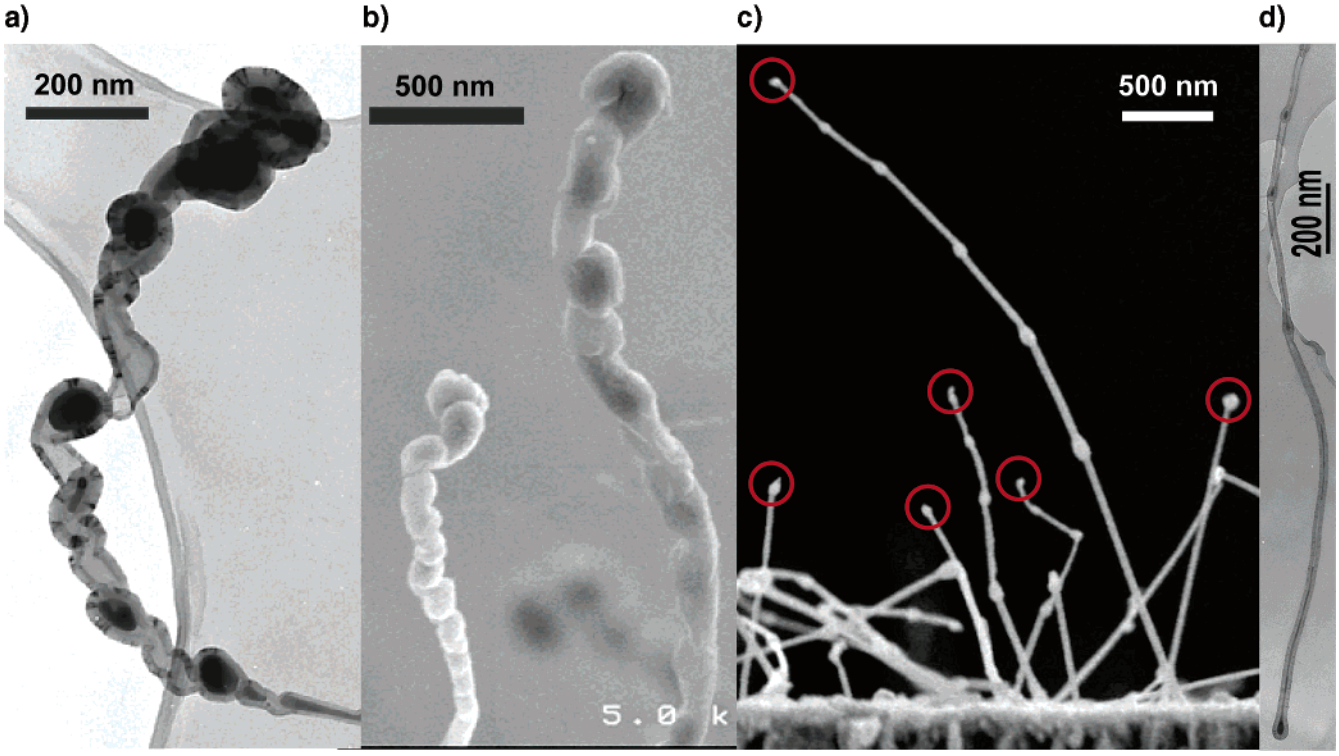

Figure 6. (a) TEM and (b) SEM images of defective filaments grown at synthesis temperatures in the range 880−1040 °C (base growth). (c) SEM and (d) TEM images of matchstick nanotubes grown at synthesis temperatures in the range 1040−1120 °C (tip growth, note the remaining catalyst particles at the tips).

Influence of the Growth Conditions. The supported catalyst used as a reference here was 64 nm Ni/15 nm Fe/anodic alumina.

a. Synthesis Temperature. Herein, the reactive gas flows were set at 100 sccm CH_4/730 sccm H_2. The SEM images in Figure 5 illustrate the results obtained in the synthesis temperature range 880−1160 °C. From 880 to 1000 °C, a high density of large and tortuous filaments is formed (Figure 5a−d). TEM and SEM revealed that these filaments present some morphological similarities with the matchstick nanotubes but with a much lower structural order (Figure 6a and b). At 1040 °C, both these defective filaments and thin, well-structured matchstick nanotubes coexist (Figure 5e). At 1080 °C, only matchstick nanotubes are formed (Figures 5f and 6c and d). Above 1120 °C, the growth activity dramatically decreases (Figure 5g and h).

A clear change of filament type is observed with the temperature: large, defective filaments below 1040 °C and thin, periodic matchstick nanotubes in the narrow range 1040−1120 °C. The two types of filaments also present an important difference in their growth mechanism: the low-temperature defective filaments grow by a base-growth mechanism, while the matchstick nanotubes grow by a tip-growth mechanism. This is illustrated by the comparison of the TEM and SEM images in Figure 6: the TEM images (Figure 6a and c) highlight the growth direction of the filaments thanks to the orientation of the included graphitic walls, while the SEM images (Figure 6b and d) show the relative orientation of the filament toward the support. The difference in base/tip-growth mode is generally explained in terms of the contact force between the catalyst particle and the substrate: weak catalyst−substrate adhesion promotes the tip-growth mode, while strong adhesive force promotes the base-growth mode.[27−29] Since the two types of filaments can be grown at the same time (i.e., experiencing the same conditions), the difference of growth mechanism can only be related to a difference of nature between the catalyst particles. EDX analyses of the particles included in the defective filaments revealed compositions quite similar to the particles included in matchstick nanotubes: ∼19 atom % P, ∼22 atom % Fe, and ∼59 atom % Ni. As a consequence, it seems likely that the difference of growth mechanism results from a difference of physical state of the catalyst particle: molten solid particles for the low temperature defective filaments and liquid particles for the high-temperature matchstick nanotubes.

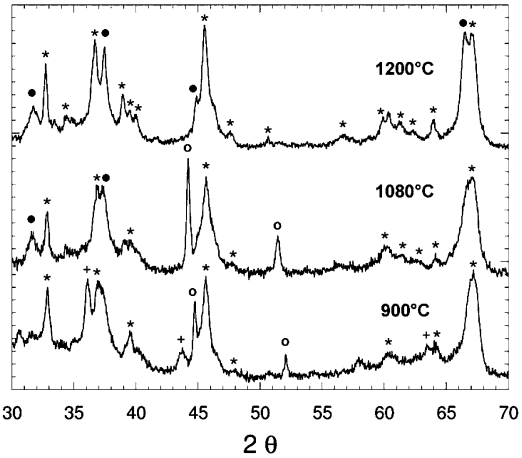

Figure 7. XRD patterns of a 64 nm Ni/15 nm Fe/anodic alumina catalyst after heat treatment at 900, 1080, and 1200 °C: alumina support (∗); fcc (Ni or Fe) (○); NiO-type oxide (+); $Ni_{12}Al_{18}O_{29}$-type aluminate (●).

The synthesis temperature influences both the nanofilament yield and morphology, while the catalyst composition only influences the yield. Using the former proposition of different eutectic temperatures inducing different catalytic activities according to the catalyst composition, we would have expected a similar catalytic behavior with the catalyst composition and the synthesis temperature. Thus, the "eutectic" explanation, at least alone, does not enable us to explain the observed catalytic

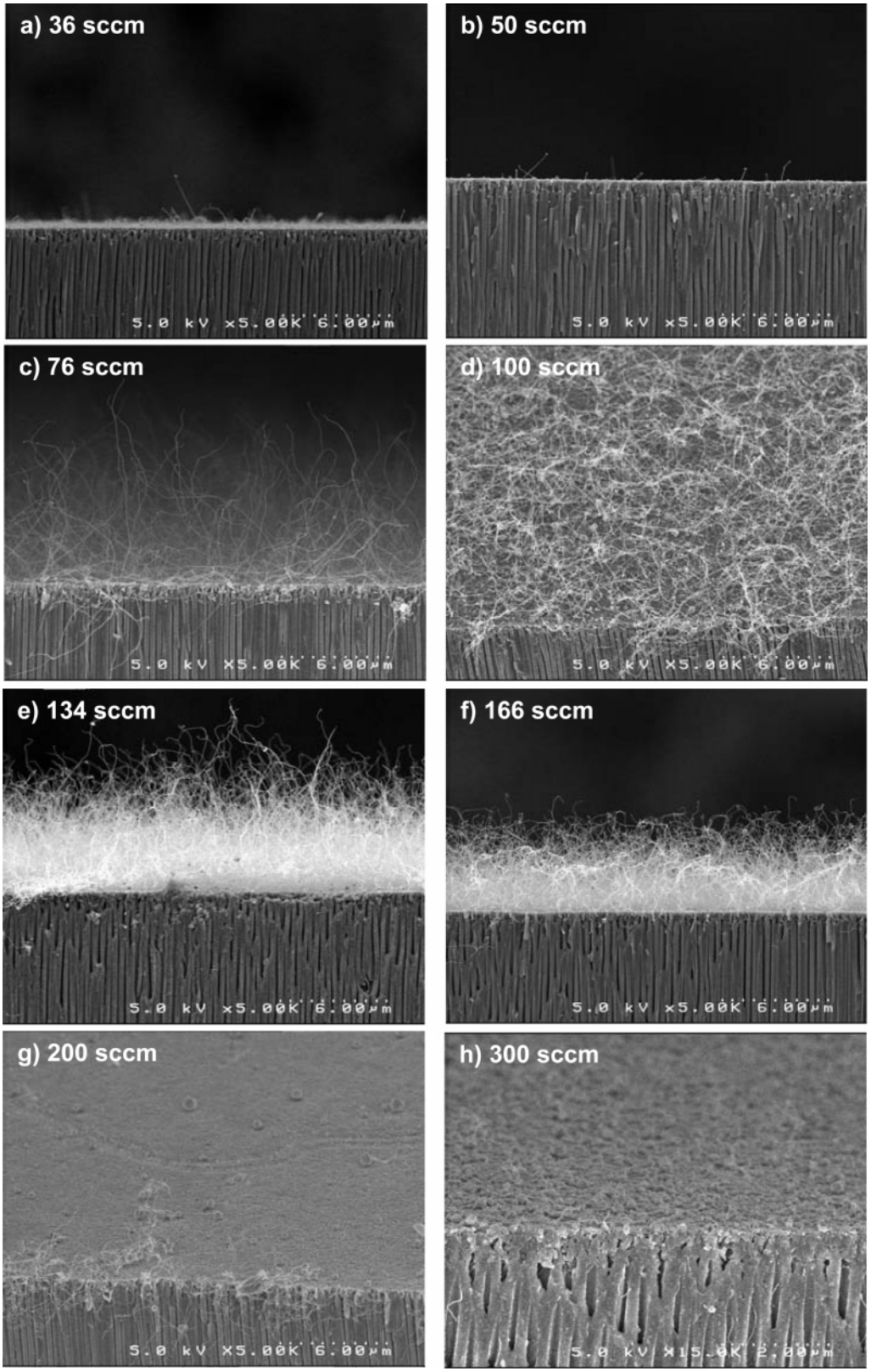

Figure 8. Postsynthesis SEM images of the substrate for different methane flow rates: 36 sccm (a); 50 sccm (b); 76 sccm (c); 100 sccm (d); 134 sccm (e); 166 sccm (f); 200 sccm (g); 300 sccm (h).

behavior. To confirm this, we investigated the structure of the catalyst layer as a function of the temperature by X-ray diffraction (XRD). Figure 7 shows the XRD patterns of a "64 nm Ni/15 nm Fe/anodic alumina" catalyst after thermal pretreatment at 900, 1080, and 1200 °C, similar to the one used before synthesis. Whatever the temperature, diffraction peaks corresponding to the alumina support crystallizing in two forms are observed. The remaining peaks correspond to the compounds formed by the Ni/Fe layer. At 900 °C, diffraction peaks characteristic of both reduced (fcc) and oxidized (NiO-type) metals are observed. At 1080 °C, fcc peaks are strongly reinforced, NiO-type peaks disappear and aluminate (Ni_{12}-$Al_{18}O_{29}$-type) peaks start appearing. At 1200 °C, fcc peaks completely disappear, while aluminate peaks are much more

intense. Whatever the temperature, no diffraction signal from (Ni or Fe) phosphide compounds could be observed. From these results, we observe that the Ni/Fe layer experiences several composition and structural changes in the range 900−1200 °C. This could account for the abrupt change of filament morphology and yield with the synthesis temperature. At the synthesis temperature found optimal for nanomatches (1080 °C), we observe that the catalyst layer is essentially in a reduced (Ni or Fe) fcc structure. However, the postsynthesis electron energy loss spectroscopy (EELS) and EDX analyses of the matchstick filaments showed that the active catalyst particles were metal phosphides, not pure metals. It is then likely that only a small fraction of the metal layer participates in the formation of the phosphide particles active for the growth. A similar XRD investigation on pure Fe deposited layers (not shown here) indicated that iron stays in an oxidized Fe_2O_3 state whatever the temperature in the range 900−1200 °C. This could explain the catalytic inefficiency of pure Fe layers, since active metal phosphides more likely form from metals in a reduced state.

b. Carbon Supply. During this study, the synthesis temperature was set at 1080 °C, the hydrogen flow rate was kept constant at 730 sccm, and the influence of the methane flow rate was studied in the range 36−300 sccm. Postsynthesis SEM images of the substrate for different methane flow rates are shown in Figure 8. Low methane flow rates (<50 sccm) induce a low density of short matchstick filaments. For methane flow rates in the range 76−166 sccm, dense entanglements of long matchstick filaments are observed. For methane flow rates higher than 200 sccm, nearly no nanostructures are observed on the surface of the substrate.

Whatever the carbon supply, only nanofilaments of the matchstick type are formed, under the growth conditions used herein. We can conclude that the influence of the synthesis temperature on the filament type does not result from the higher carbon supplies/activities at higher temperatures, since the carbon supply has no influence on the filament type. However, we observed that the carbon supply strongly influences the filament yield. Weak catalytic activities at low carbon supply could result from carbon activities too low to reach the carbon supersaturation of the catalyst particles, which is needed to initiate the growth. The absence of activity at high methane flow rates could result from the poisoning of the surface of the catalyst particles by amorphous carbon. Further evidences are needed to clarify this.

Conclusion

Several important aspects have to be considered to grow matchstick nanotubes by sequential catalytic growth. Metal phosphide catalyst nanoparticles are needed to initiate a sequential growth mechanism. Phosphorus can be present in the catalyst support or added by phosphoric acid impregnation. The phosphide particles are likely to be in a liquid state during the growth: this is supported by (a) the necessary fluid state of the catalyst particles included during the growth, (b) the abrupt appearance from 1040 °C of much smaller catalyst particles (active for the growth of matchstick nanotubes), and (c) the change of mechanism from base growth to tip growth at 1040 °C. XRD investigations indicated that the deposited layer can form different compounds (pure metal, oxides, and aluminates) as a function of the temperature and the metal composition. This can be correlated with the strong influence of the metal composition on the nanofilament yield and with the narrow temperature range enabling the selective growth of matchstick nanotubes. At the optimal synthesis temperature, most of the deposited metal layer is observed to be in a reduced state. The catalytically active metal phosphide is likely to be a minority phase forming small and isolated nanoparticles from the surface of this reduced metal layer. The carbon supply strongly influences the nanofilament yield but does not affect the nanofilament type. This, again, confirms that controlling the nature of the catalyst particles (composition, size, and physical state) is the crucial step for inducing sequential growth and for synthesizing matchstick nanotubes.

Acknowledgment. This work was partially financed by EU projects COMELCAN (no. HPRN-CT-2000-00128) and FUNCARS (no. HPRN-CT-1999-00011).

References and Notes

(1) de Heer, W. A.; Chatelain, A.; Ugarte, D. *Science* **1995**, *270*, 1179.
(2) Fan, S.; Chapline, M. G.; Franklin, N. R.; Tombler, T. W.; Cassel, A. M.; Dai, H. *Science* **1999**, *283*, 512.
(3) Frank, S.; Poncharal, P.; Wang, Z. L.; de Heer, W. A. *Science* **1998**, *280*, 1744.
(4) Tsukagoshi, K.; Alphenaar, B. W.; Ago, H. *Nature* **1999**, *401*, 572.
(5) Buitelaar, M. R.; Bachtold, A.; Nussbaumer, T.; Iqbal, M.; Schönenberger, C. *Phys. Rev. Lett.* **2002**, *88*, 156801.
(6) Baughman, R. H.; Cui, C.; Zakhidov, A. A.; Iqbal, Z.; Barisci, J. N.; Spinks, G. M.; Wallace, G. G.; Mazzoldi, A.; de Rossi, D.; Rinzler, A. G.; Jaschinski, O.; Roth, S.; Kertesz, M. *Science* **1999**, *284*, 1340.
(7) Kim, P.; Lieber, C. M. *Science* **1999**, *286*, 2148.
(8) Service, R. F. *Science* **2001**, *292*, 45.
(9) Wolf, S. A.; Awscalom, D. D.; Buhrman, R. A.; Daughton, J. M.; von Molnàr, S.; Roukes, M. L.; Chtchelkanova, A. Y.; Treger, D. M. *Science* **2001**, *294*, 1488.
(10) Yang, C.-K.; Zhao, J.; Lu, J. P. *Phys. Rev. Lett.* **2003**, *90*, 257403.
(11) Kuo, C. T.; Lin, C. H.; Lo, A. Y. *Diamond Relat. Mater.* **2003**, *12*, 799.
(12) Dujardin, E.; Ebbesen, T.; Hiura, H.; Tanigaki, K. *Science* **1994**, *265*, 1850.
(13) Pederson, M. R.; Broughton, J. Q. *Phys. Rev. Lett.* **1992**, *69*, 2689.
(14) Seraphin, S.; Zhou, D.; Jiao, J.; Withers, J. C.; Loufty, R. *Nature* **1993**, *362*, 503.
(15) Ajayan, P. M.; Colliex, C.; Lambert, J. M.; Bernier, P.; Barbedette, L.; Tence, M.; Stephan, O. *Phys. Rev. Lett.* **1994**, *72*, 1722−1725.
(16) Guerret-Piécourt, C.; Le Bouar, Y.; Loiseau, A.; Pascard, H. *Nature* **1994**, *372*, 761.
(17) Hsu, W. K.; Hare, J. P.; Terrones, M.; Kroto, H. W.; Walton, D. R. M. *Nature* **1995**, *377*, 687.
(18) Liang, C. H.; Meng, G. W.; Zhang, L. D.; Shen, N. F.; Zhang, X. Y. *J. Cryst. Growth* **2000**, *218*, 136.
(19) Sinha, A. K.; Hwang, D. W.; Hwang, L.-P. *Chem. Phys. Lett.* **2000**, *332*, 455.
(20) Ajayan, P. M.; Ebbesen, T.; Ichihashi, T.; Iijima, S.; Tanigaki, K.; Hiura, H. *Nature* **1993**, *362*, 522.
(21) Ajayan, P. M.; Iijima, S. *Nature* **1993**, *361*, 333.
(22) Tsang, S. C.; Chen, Y. K.; Harris, P. J. F.; Green, M. L. H. *Nature* **1994**, *372*, 159.
(23) Loiseau, A.; Willaime, F. *Appl. Surf. Sci.* **2000**, *164*, 227.
(24) Jourdain, V.; Kanzow, H.; Castignolles, M.; Loiseau, A.; Bernier, P. *Chem. Phys. Lett.* **2002**, *364*, 27.
(25) Jourdain, V.; Stéphan, O.; Castignolles, M.; Loiseau, A.; Bernier, P. *Adv. Mater.* **2004**, *16*, 447.
(26) Massalski, T. B. *Binary Alloy Phase Diagrams*, 2nd ed.; ASM International: The Materials Information Society, 1990.
(27) Tibbetts, G. G. *J. Cryst. Growth* **1984**, *66*, 632.
(28) Baker, R. T. K. *Carbon* **1989**, *27*, 315.
(29) Song, I. K.; Cho, Y. S.; Choi, G. S.; Park, J. B.; Kim, D. J. *Diamond Relat. Mater.* **2004**, *13*, 1210.